COMPUTATION OF BLOOD FLOW IN THE LEFT VENTRICLE WITH FLUID-STRUCTURE INTERACTION

Matthew G. Doyle
Department of Mechanical Engineering
University of Ottawa
161 Louis Pasteur, Ottawa, Ontario K1N 6N5 Canada
mdoyl009@uottawa.ca

Stavros Tavoularis
Department of Mechanical Engineering
University of Ottawa
161 Louis Pasteur, Ottawa, Ontario K1N 6N5 Canada
stavros.tavoularis@uottawa.ca

Yves Bourgault
Department of Mathematics and Statistics
University of Ottawa
585 King Edward, Ottawa, Ontario K1N 6N5 Canada
ybourg@uottawa.ca

ABSTRACT

This paper describes the results of a simulation of blood flow and myocardium motion in an average canine left ventricle (LV) with fluid-structure interaction. The computed LV cavity pressure was in fair agreement with previous measurements over most of the cardiac cycle; however, during rapid filling, the calculated pressure was lower than the measured one, which led to non-physiological backflow. Trends of LV cavity volume changes were nearly physiological for three of the four phases of the cardiac cycle but the ejection fraction was lower than physiological. This method predicts appreciable pressure variations in the LV cavity, in contrast to solid-only simulations which assume uniform cavity pressure. The dependence of the results on various model parameters is briefly discussed along with suggestions for future work.

INTRODUCTION

Numerical simulations of the mechanics of the heart require the use of models for both the deformation of the solid wall and the flow of blood as well as a mechanism for coupling the two, namely fluid-structure interaction (FSI). Previous FSI simulations of the heart (Peskin and McQueen, 1996; Watanabe et al., 2004; Krittian et al., 2010) have made many simplifying assumptions in their solid mechanics models and, although predicting realistic blood flow patterns, were of limited success in simulating accurately the stress-strain behaviour of the wall.

The objective of the present study was to perform FSI simulations of the mechanics of an average canine left ventricle (LV) over the full cardiac cycle. In earlier phases of this project, we have developed a material model for the myocardium (Doyle et al., 2010) and generated a set of initial conditions which are suitable for cardiac cycle simulations (Doyle et al., 2011). As part of the third phase of this study, this article reports results of these simulations over the cardiac cycle.

METHODS

Geometry and Mesh

The solid and fluid geometries in this work are idealized and have been defined in their reference states to be representative of an average canine LV at diastasis, which is the middle phase of ventricular filling (diastole). The solid geometry was defined as a truncated prolate ellipsoid (i.e., a solid generated by an ellipse that has been revolved around its major axis), as shown in Figure 1a, with dimensions a = 46.92 mm, b = 27.84 mm, t_a = 6.83 mm, t_b = 12.42 mm, and h = 60.14 mm. The fluid geometry, shown in Figure 1b, consists of two parts; a lower part, for which the outer surface matches the inner surface of the solid geometry, and an upper part, consisting of two cylindrical tubes, which represent the LV inflow and outflow tracts, and a section of a sphere, which caps the truncated ellipsoid. The dimensions of the upper part of the fluid geometry were D_{AV} = 9.78 mm, D_{MV} = 18.88 mm, L_1 = 9.78 mm, L_2 = 7.78 mm, w_1 = 26.71 mm, α = 60°, β = 75°, and θ = 135°.

The solid geometry was meshed using ten-node tetrahedral elements, whereas the fluid was meshed using four-node tetrahedral elements, both on unstructured grids, as shown in Figure 2. Simulations were performed for the finest solid

mesh for which solution convergence could be achieved. Although our previous solid-only simulations (Doyle et al., 2011) demonstrated the need for solid mesh refinement, this was not possible at present because of solution divergence. For the fluid, results obtained using two different meshes were in good agreement; fluid mesh refinement seems also to be desirable, but this was not presently feasible, as it would increase substantially the computational time.

Numerical Methods

Simulations in this work were performed on the computing clusters of the High Performance Computing Virtual Laboratory (HPCVL) using the commercial finite element software ADINA v. 8.5.2 (ADINA R & D, Inc., Watertown, MA, USA).

The myocardium, which is the thick middle layer of the heart wall and the only layer considered in this study, was modelled as undergoing large displacements for large strains and was simulated using the Total Lagrangian form of the appropriate governing equation, defined as

$$\begin{aligned}&\mathbf{M}\ddot{\mathbf{U}}(t+\Delta t)+\mathbf{C}\dot{\mathbf{U}}(t+\Delta t)+\mathbf{K}(t)[\mathbf{U}(t+\Delta t)-\mathbf{U}(t)]\\&=\mathbf{R}(t+\Delta t)-\mathbf{F}(t)\end{aligned} \quad (1)$$

where $\mathbf{U}$, $\dot{\mathbf{U}}$, and $\ddot{\mathbf{U}}$ are the nodal displacement, velocity and acceleration vectors, respectively, $\mathbf{M}$ is the mass matrix, $\mathbf{C}$ is the damping matrix, $\mathbf{K}$ is the stiffness matrix, $\mathbf{R}$ is the external load vector, $\mathbf{F}$ is the force vector equivalent to the element stresses, and t is time (ADINA R & D, Inc., 2008a).

The myocardium was modelled as a transversely isotropic material with properties that differed in the directions parallel and perpendicular to the muscle fibres. This material model was defined by a strain energy density function W, consisting of two parts, passive W_p and active W_a. The passive part modelled the stress-strain behaviour of the myocardium when the muscle fibres were relaxed, and the active part provided additional stresses to model the contraction of the muscle fibres. The sum of the two parts models the total stress state, defined as

$$W = W_p + W_a \quad (2)$$

where

$$W_p = C_1\left(e^Q - 1\right) + \tfrac{1}{2}\kappa_s\left(J_3 - 1\right)^2 \quad (3)$$

$$Q = C_2\left(J_1 - 3\right)^2 + C_3\left(J_1 - 3\right)\left(J_4 - 1\right) + C_4\left(J_4 - 1\right)^2 \quad (4)$$

$$\begin{aligned}W_a = {} & D_0 + D_1\left(J_1 - 3\right)\left(J_4 - 1\right) + D_2\left(J_1 - 3\right)^2 \\ & + D_3\left(J_4 - 1\right)^2 + D_4\left(J_1 - 3\right) + D_5\left(J_4 - 1\right)\end{aligned} \quad (5)$$

In Eqs. (3) to (5), C_i and D_i are passive and active material parameter values, respectively, κ_s is the bulk modulus, which governs the material compressibility, and J_i are reduced invariants of Green's strain tensor $\mathbf{E}$.

The contraction and relaxation of the muscle fibres during the cardiac cycle were modelled by the gradual application and removal of the active stresses, which was modelled by varying D_i using the following equation

$$D_i = FD_{i,\max} \quad (6)$$

where F is a forcing function which varies from 0 when the muscle fibres are fully relaxed to 1 when the muscle fibres are fully contracted and $D_{i,\max}$ are the values of D_i for $F = 1$. F is defined by sigmoid functions during the four phases of the cardiac cycle and is shown in Figure 3 as a function of the dimensionless time τ, which is time normalized by the period.

As shown in Figure 1a, the myocardium has been subdivided into six layers, each with its own muscle fibre orientation; fibres are inclined with respect to the local circumferential direction by angles in the range from -60° to +60° from the outer layer to the inner layer.

Blood was assumed to be a slightly compressible Newtonian fluid and its flow in the LV was assumed to be laminar. The choice of a slightly compressible fluid instead of an incompressible one was made to ensure convergence at instances when both inflow and outflow valves are closed and the geometry is deforming. Simulations were performed using the following arbitrary-Lagrangian-Eulerian (ALE) forms of the continuity and momentum equations for slightly compressible fluids, which account for the velocity of the moving mesh

$$\frac{\rho_f}{\kappa_f}\left(\frac{\partial p}{\partial t} + \left(\boldsymbol{v} - \boldsymbol{w}\right)\cdot\nabla p\right) + \rho_m \nabla\cdot\boldsymbol{v} = 0 \quad (6a)$$

$$\rho_f \frac{\partial \boldsymbol{v}}{\partial t} + \rho_f\left(\boldsymbol{v} - \boldsymbol{w}\right)\cdot\nabla\boldsymbol{v} - \nabla\cdot\boldsymbol{\sigma}_f = \boldsymbol{f}^B \quad (6b)$$

In these equations, p is pressure, $\boldsymbol{v}$ is the velocity vector, $\boldsymbol{w}$ is the mesh velocity vector, ρ_m is the density of the compressible fluid, $\boldsymbol{\sigma}_f$ is the stress tensor, and $\boldsymbol{f}^B$ is the body force per unit volume (ADINA R & D, Inc., 2008b).

Flow in the system was driven by the deformation of the myocardium coupled with the application of left atrial (LA) and aortic (Ao) pressure boundary conditions; these pressures, shown in Figure 4, were defined based on previous measurements (Sabbah and Stein, 1981), and were applied to the distal ends of the LV inflow and outflow tracts, respectively. Flow direction was controlled by instantly opening and closing planar inflow (mitral) and outflow (aortic) valves located near the proximal ends of the inflow and outflow tracts. The opening and closing of these valves was controlled by time functions, which were applied to match the timing of the pressure boundary conditions.

Initial conditions for both the fluid and the solid models were required to start the cardiac cycle simulations. We chose to start the simulations at end diastole, because at this instant both valves are closed and the muscle fibres are fully relaxed. To generate an initial end-diastolic state with non-zero stresses in the myocardium, we inflated our initial reference geometry, defined at diastasis, by a static pressure load to an end-diastolic pressure (Doyle et al., 2011). Because the muscle fibres are fully relaxed during the period between diastasis and end diastole, only the passive part of the myocardium material model was required during this inflation. Simulations were started from end diastole and proceeded through the four phases of the cardiac cycle, namely isovolumetric contraction (IVC), ejection, isovolumetric relaxation (IVR), and filling.

RESULTS

Simulations were performed for two periods of the cardiac cycle. Plots of the temporal variations of the LV pressure p_{LV} and the LV cavity volume V_f over these two periods are presented in Figures 4a and b, respectively, and the variations of p_{LV} versus V_f are presented in Figure 5. The temporal variations of p_{LV} show good agreement with previous measurements over the majority of the cardiac cycle. However, during rapid filling, when $0.385 \leq \tau \leq 0.650$, the calculated p_{LV} exceeded the measured value as well as p_{LA}, which caused non-physiological backflow in this region. Spikes in p_{LV}, particularly visible in period 2, correspond to times for which a valve closed and are attributed to the assumption of instantly opening and closing planar valves made in the present simulations. FSI modelling of natural heart valves would have probably alleviated these problems, but, besides the technical challenges that this would pose, it would have added considerably to the computational time required for the simulations.

In Figure 4b, small changes in V_f were visible during IVC, which is a phase in the cardiac cycle during which the muscle fibres are contracting, both valves are closed, and no blood should enter or exit the LV cavity. In the present study, these volume changes were attributed to the use of the slightly compressible model for blood, as required to ensure model convergence during the isovolumetric phases. During ejection, blood exited the LV cavity as shown by the decrease in V_f during this phase. The change in V_f during ejection can be characterized by the ejection fraction, defined as $EF = (V_{f,ED} - V_{f,ES})/V_{f,ED}$, where the subscripts ED and ES denote end diastole and end systole, respectively. In the present study, we found $EF = 0.081$ for period 1 and 0.084 for period 2, which are lower than the physiological value of approximately 0.44 for a canine LV (Bovendeerd et al., 1996; Kerckhoffs et al., 2007). As with IVC, small changes in V_f were visible during IVR. Lastly, during rapid filling, V_f increased dramatically, exceeding its end-diastolic value, before non-physiological backflow caused V_f to decrease. During the latter part of filling, V_f increased and decreased during both periods, but reached end-diastolic values that were approximately 98% of the starting value for period 1 and approximately 99% of the starting value for period 2. From this, we can conclude that the non-physiological backflow did not affect significantly the near-conservation of the LV cavity volume for each period.

In Figure 5, the trends of p_{LV} versus V_f for the first three phases of the cardiac cycle were consistent with physiological expectations, whereas backflow prevented the filling trends from meeting expectations. For period 2, the overall trends were comparable to period 1, with differences primarily due to differences in V_f during the isovolumetric phases.

Figures 6 and 7 show pressure contour plots and velocity vectors in the y-z centreplane for the two periods at end systole and end diastole, respectively. Pressures in the LV cavity at end systole are large compared to the pressures at end diastole. Pressure variations near the LV outflow tract at end systole can be attributed to the sudden closing of the aortic valve, as discussed previously. Within the LV cavity, for period 1, p_{LV} increased from 14.4 kPa at the apex to 15.6 kPa at the centre of the basal plane (top plane in the deformable part of the fluid geometry); for period 2, p_{LV} increased from 11.6 kPa at the apex to 20.0 kPa at the basal plane. The variations of pressure within the LV cavity show the importance of performing FSI simulations of the mechanics of the LV rather than solid-only simulations with assumed uniform pressure boundary conditions from the fluid. At end diastole, non-uniform pressures are visible in the contours in Figure 7, although the magnitudes of these pressure variations are smaller than at end systole.

Velocity vectors at end systole differ from period 1 to period 2, with much larger velocities visible for period 2, particularly near the apex, which is deforming downwards. At end diastole, the velocity vectors were found to be larger for period 1 than for period 2.

Average Reynolds numbers were calculated for systole and diastole as (Krittian et al., 2010) $\mathrm{Re} = \rho_f v D/\mu$, where v is the characteristic velocity and D is the characteristic diameter; $D = D_{AV}$, $\bar{v} = \Delta V_{f,eject} \Big/ \left((0.6 \Delta \tau_{eject}) \pi (D_{AV}/2)^2 \right)$ for systole, $D = D_{MV}$, $\bar{v} = \Delta V_{f,fill} \Big/ \left((0.6 \Delta \tau_{fill}) \pi (D_{MV}/2)^2 \right)$ for diastole. Using these definitions, for periods 1 and 2, respectively, Re = 1749 and 2941 for systole and Re = 193 and 359 for diastole. The calculated Reynolds numbers would most likely increase with increasing ejection fraction. It happens that, for period 2, the systolic Re is comparable to the value of 3431 calculated by Krittian et al. (2010) for a human LV, although one should keep in mind that quantitative comparisons are not appropriate between species because of different pulsation rates and LV sizes. For diastole, Krittian et al. (2010) found Re = 2288, which is much larger than the values calculated in the present study, although this is also subjected to the same reservations.

DISCUSSION

In this section, we discuss the successes and limitations of the present study along with future directions and challenges in the modelling of the mechanics of the LV with FSI effects.

Simulations in the present study were performed using an average canine LV geometry, rather than a specimen-specific one due to the difficulty in obtaining all necessary model inputs for a single specimen and the variability in the values of these inputs from one specimen to the next. The determination of average valve diameters was subject to considerable uncertainty. Considering that the computed ejection fraction was lower than the physiological range, it seems that the present choices of the LV outflow and inflow tract diameters may be, respectively, too low and too high. This conjecture is further supported by the fact that the ratio of systolic to diastolic Re in the present study was approximately 9 for period 1 and 8 for period 2, in both cases much higher than the value 1.5 for the human LV (Krittian et al., 2010). Increasing D_{AV} and decreasing D_{MV} may serve to decrease the systolic Reynolds number and increase the diastolic one, which would in turn decrease the ratio of the two. In

summary, adjustments in LV inflow and outflow tract diameters may be appropriate for future studies. Additionally, the assumption of rigid inflow and outflow tracts could also be revisited subject to the availability of measurements of the muscle fibre angles, wall thicknesses, and material properties in this region.

The non-physiological backflow into the LV cavity during filling may be attributed to insufficient muscle fibre relaxation during rapid filling, crudeness of the boundary conditions, and/or absence of a model for the valve dynamics. During rapid filling, the completion of the muscle fibre relaxation causes a decrease in p_{LV} even though fluid is entering the LV. For the current study, the forcing function $F(\tau)$ controls the relaxation of the muscle fibres; unfortunately, none of the many assumed forms of this function was successful in producing sufficient fibre relaxation during rapid filling to prevent backflow. Perhaps other, yet unspecified, forms of $F(\tau)$ might alleviate this problem. In the present study, pressure boundary conditions were used to drive the flow at the inlet and outlet of the LV model. An alternative approach would have been to couple the finite element model with electric circuit models to represent the circulatory system upstream and downstream of the LV. This approach has been followed by other researchers, and could be implemented in extensions of the present study, albeit by adding appreciable complexity to the numerical model. As previously discussed, spikes in p_{LV} were visible when the valves were abruptly closed. Modelling the dynamics of valve motion, especially when coupled with a deformable LV geometry and FSI effects, remains a challenging problem. In fact, only recently (Wenk et al., 2010) has a solid-only model been developed consisting of LV deformation coupled with the motion of the mitral valve. Much work is still required to extend this model to include aortic valve motion and FSI effects.

CONCLUSIONS

Complete numerical simulations of the mechanics of the canine LV have been successfully performed for two periods of the cardiac cycle. Calculated LV cavity pressures showed good agreement with previous measurements for most of the cycle, but differed during rapid filling, when non-physiological backflow occurred. Trends in LV cavity volume variation were consistent with expectations for IVC, ejection, and IVR, but the calculated ejection fraction was smaller than physiological values. Pressure variations throughout the LV cavity at end systole and end diastole show the importance of including FSI effects rather than performing solid-only simulations with a prescribed uniform pressure boundary condition from the fluid. Lastly, the dependence of the results upon several model inputs was discussed along with suggestions for model improvements in future studies.

REFERENCES

ADINA R & D, Inc., 2008, *Theory and Modeling Guide, Volume I: ADINA. Report ARD 08-7*. ADINA R & D, Inc., Watertown, MA.

ADINA R & D, Inc., 2008, *Theory and Modeling Guide, Volume III: ADINA CFD & FSI. Report ARD 08-9*. ADINA R & D, Inc., Watertown, MA.

Bovendeerd, P. H. M., Arts, T., Delhaas, T., Huyghe, J. M., van Campen, D. H., and Reneman, R. S., 1996, "Regional Wall Mechanics in the Ischemic Left Ventricle: Numerical Modeling and Dog Experiments," *American Journal of Physiology*, Vol. 270, pp. H398-H410.

Doyle, M. G., Tavoularis, S., and Bourgault, Y., 2010, "Adaptation of a Rabbit Myocardium Material Model for Use in a Canine Left Ventricle Simulation Study", *ASME Journal of Biomechanical Engineering*, Vol. 132, pp. 041006-01-12.

Doyle, M. G., Tavoularis, S., and Bourgault, Y., 2011, "Simulation of the Static Inflation of the Passive Left Ventricle to an End Diastolic State", (submitted for publication).

Kerckhoffs, R. C. P., Neal, M. L., Gu, Q., Bassingthwaighte, J. B., Omens, J. H., and McCulloch, A. D., 2007, "Coupling of a 3D Finite Element Model of Cardiac Ventricular Mechanics to Lumped Systems Model of the Systemic and Pulmonic Circulation," Annals of Biomedical Engineering, Vol. 35, pp. 1-18.

Krittian, S., Janoske, U., Oertel, H., and Böhlke, T., 2010, "Partitioned Fluid-Solid Coupling for Cardiovascular Blood Flow", *Annals of Biomedical Engineering*, Vol. 38, pp. 1426-1441.

Peskin, C. S., and McQueen, D. M., 1996, "Fluid Dynamics of the Heart and its Valves," *Case Studies in Mathematical Modeling - Ecology, Physiology, and Cell Biology*, H. G. Othmer, et al., ed., Prentice-Hall, Inc., Englewood Cliffs, NJ, pp. 309-337.

Sabbah, H. N., and Stein, P. D., 1981, "Pressure-Diameter Relations during Early Diastole in Dogs: Incompatibility with the Concept of Passive Left Ventricular Filling," *Circulation Research*, Vol. 45, pp. 357-365.

Watanabe, H., Sugiura, S., Kafuku, H., and Hisada, T., 2004, "Multiphysics Simulation of Left Ventricular Filling Dynamics Using Fluid-Structure Interaction Finite Element Method", *Biophysical Journal*, Vol. 87, pp. 2074-2085.

Wenk, J. F., Zhang, Z., Cheng, G., Malhotra, D., Acevado-Bolton, G., Burger, M., Suzuki, T., Saloner, D. A., Wallace, A. W., Guccione, J. M., and Ratcliffe, M. B., 2010, "First Finite Element Model of the Left Ventricle With Mitral Valve: Insights Into Ischemic Mitral Regurgitation," *Annals of Thoracic Surgery*, Vol. 89, pp. 1546-1554.

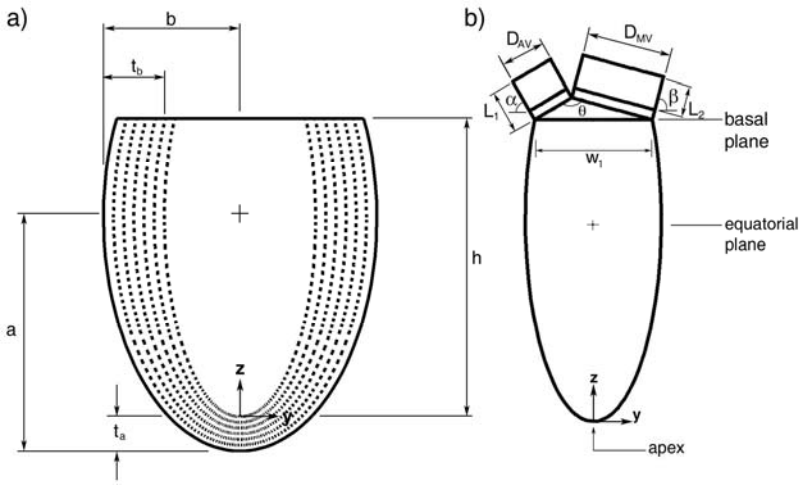

Figure 1. Solid (a) and fluid (b) geometries with key dimensions and geometric landmarks.

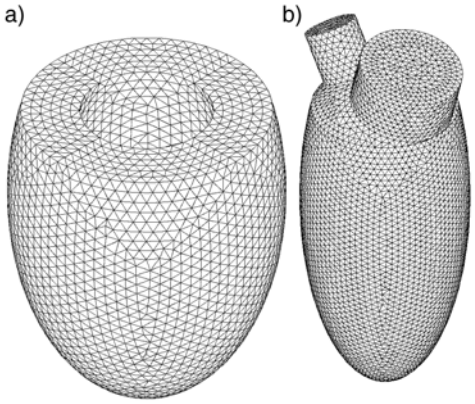

Figure 2. Solid (a) and fluid (b) meshes.

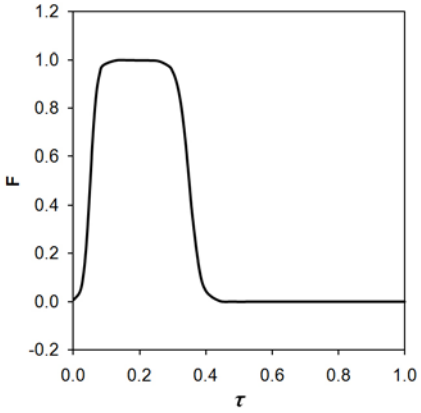

Figure 3. Forcing function.

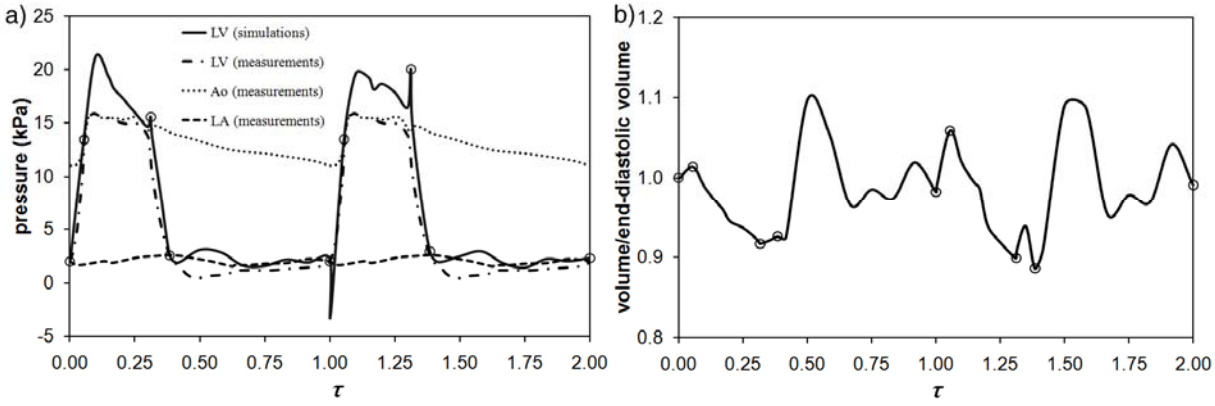

Figure 4. a) Temporal variation of pressures and b) temporal variations of LV cavity volume. In this and subsequent figures, circles denote the opening or closing of a valve and the start of a phase of the cardiac cycle.

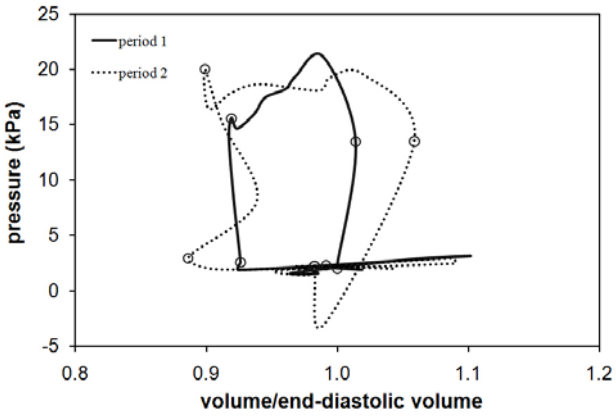

Figure 5. Variation of LV pressure as a function of LV cavity volume.

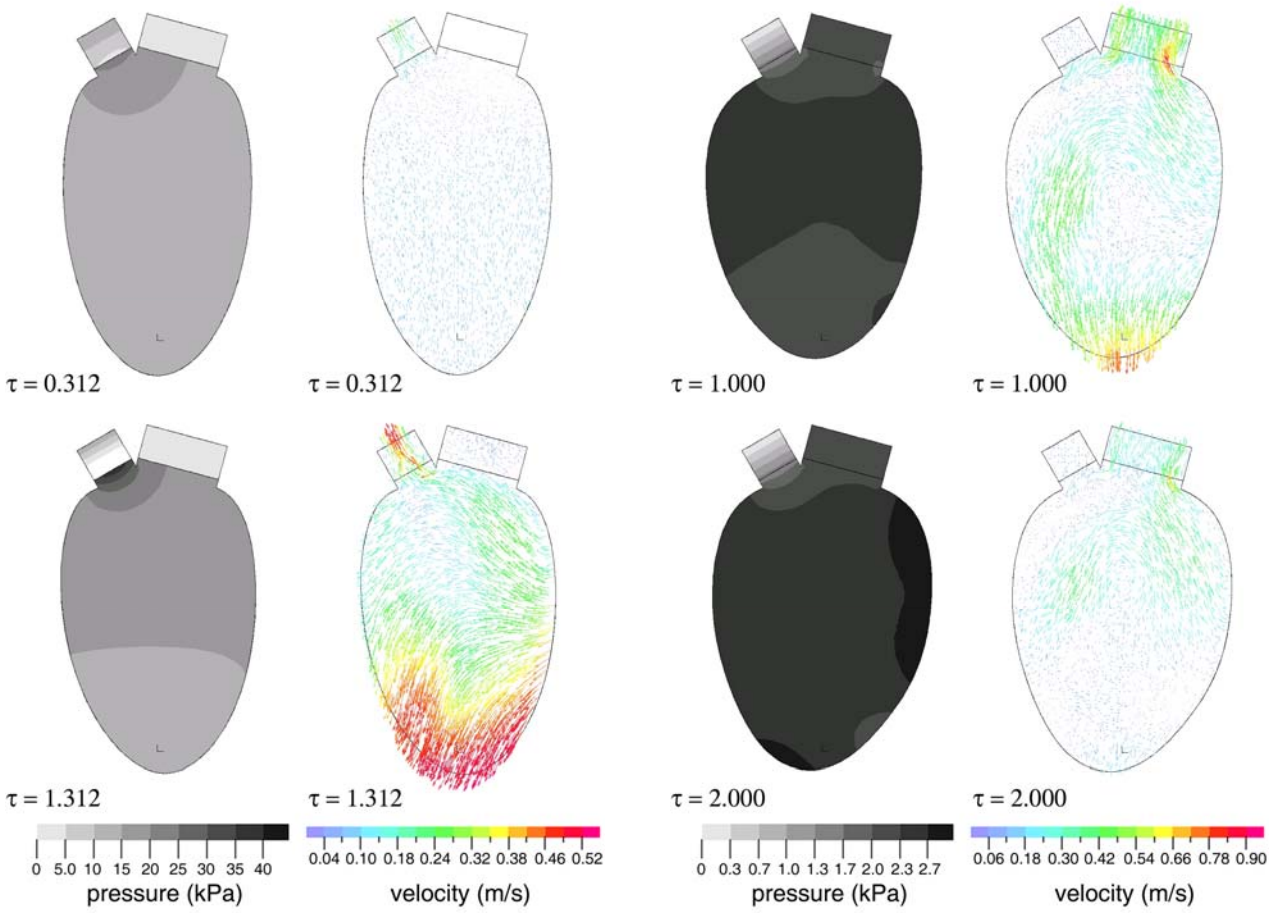

Figure 6. LV cavity pressure contours and velocity vector maps in the *y*-*z* centreplane at end systole for two periods.

Figure 7. LV cavity pressure contours and velocity vector maps in the *y*-*z* centreplane at end diastole for two periods.